Near-source Doppler radar monitoring of tephra plumes at Etna

F. Donnadieu, P. Freville, C. Hervier, M. Coltelli, S. Scollo, M. Prestifilippo,
S. Valade, S. Rivet, P. Cacault

Near-source Doppler radar monitoring of tephra plumes at Etna

F. Donnadieu [a,b,c,d,*],

P. Freville [d], C. Hervier [d], M. Coltelli [e], S. Scollo [e], M. Prestifilippo [e], S. Valade [a,b,c,1], S. Rivet [d], P. Cacault [d]

[a] Clermont Université, Université Blaise Pascal, Laboratoire Magmas et Volcans, BP 10448, F-63000 Clermont-Ferrand, France

[b] CNRS, UMR 6524, LMV, F-63038 Clermont-Ferrand, France

[c] IRD, R 163, LMV, F-63038 Clermont-Ferrand, France

[d] CNRS, UMS 833, OPGC, F-63177 Aubiere, France

[e] Istituto Nazionale di Geofisica e Vulcanologia, Osservatorio Etneo, sezione di Catania (INGV-OE), Italy

[*] Corresponding author.

[1] Now at Dipartimento di Scienze della Terra, Università di Firenze, Firenze — Italy.

Abstract

Over the last twenty years Mount Etna has produced more than one hundred explosive events ranging from light ash emissions to violent sub-plinian eruptions. Significant hazards arise from tephra plumes which directly threaten air traffic, and generate fallout affecting surrounding towns and infrastructures. We describe the first radar system, named VOLDORAD 2B, fully integrated into a volcano instrumental network dedicated to the continuous near-source monitoring of tephra emissions from Etna's summit craters. This 23.5 cm wavelength pulsed Doppler radar is operated in collaboration between the Observatoire de Physique du Globe de Clermont-Ferrand (OPGC) and the Istituto Nazionale di Geofisica e Vulcanologia, Osservatorio Etneo (INGV-OE) since 2009. Probed volumes inside the fixed, northward-pointing conical beam total about 1.5 km in length, covering the summit craters which produced all recent tephra plumes. The backscattered power, related to the amount of particles crossing the beam, and particle along-beam velocities are recorded every 0.23 s, providing a proxy for the tephra mass eruption rate. Radar raw data are transmitted in real-time to the volcano monitoring center of INGV-OE in Catania and are used to automatically release alerts at onset and end of eruptive events. Processed radar parameters are also made available from the VOLDORAD database online (http://voldorad.opgc.fr/). In addition to eruptive crater discrimination by range gating, relative variations of eruption intensity can be tracked, including through overcast weather when other optical or infrared methods may fail to provide information. Short-lived dense ash emissions can be detected as illustrated for weak ash plumes from the Bocca Nuova and New South East craters in 2010. The comparison with thermal images suggests that the front mushroom of individual ash plumes holds the largest particles (coarse ash and small lapilli) and concentrations at least within the first hundred meters. For these short-lived ash plumes, the highest particle mass flux seems to occur typically within the first 10 s. We also analyze data from the first lava fountain generating an ash and lapilli plume on 12 January 2011 that initiated a series of 25 paroxysmal episodes of the New South East Crater until April 2012. We illustrate the pulsating behavior of the lava fountain and show that vertical velocities reached 250 m s^{-1} (with brief peaks exceeding 300 m s^{-1}), leading to mean and maximum tephra fluxes (DRE) of 185 and 318 m^3 s^{-1} (with peaks exceeding 380 m^3 s^{-1}) respectively, and a total volume of pyroclasts emitted during the lava fountain phase of 1.3×10^6 m^3. Finally, we discuss capacities and limits of the instrument, along with future work aimed at providing source term inputs to tephra dispersal models in order to improve hazard assessment and risk mitigation at Etna.
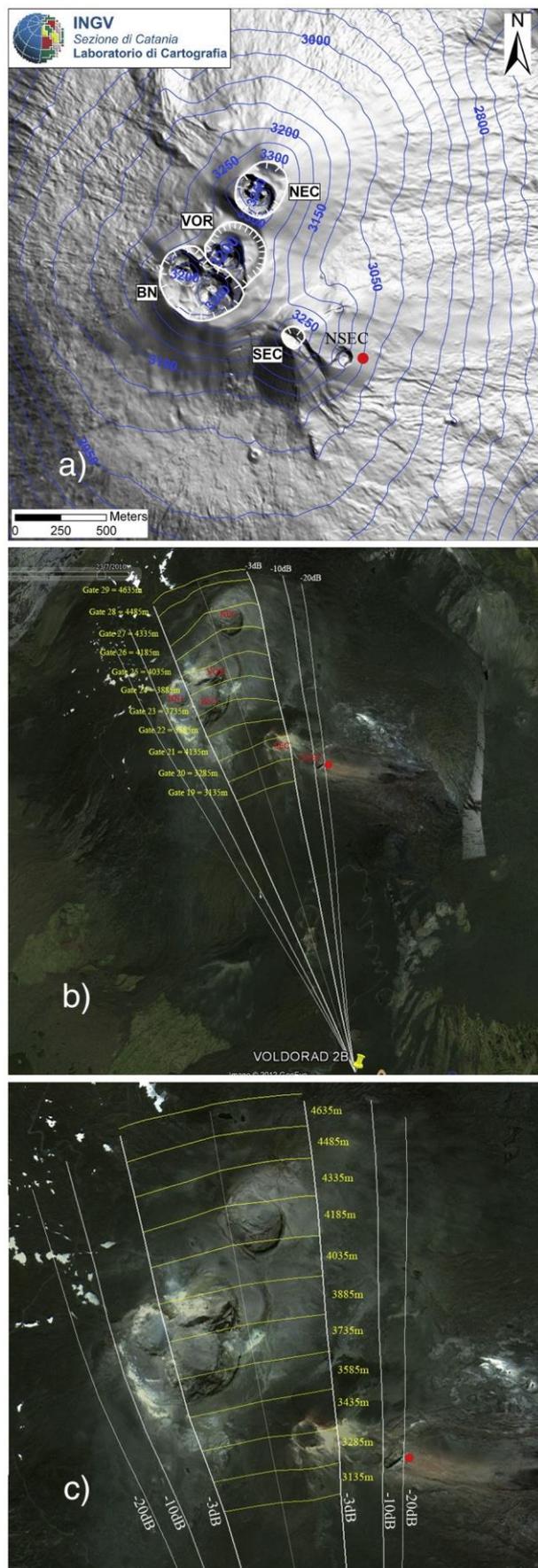
Keywords: Doppler radar, Mount Etna, New South East Crater, Real-time monitoring, VOLDORAD database, Tephra plume hazard

1. Introduction

1.1. Volcanic ash plume hazards at Etna

Etna has produced more than 200 violent explosive events since 1979, with fire fountains that formed eruptive columns from 5 to 15 km a.s.l. and erupted tephra volumes from 10^4 to 10^7 m^3 (Branca and Del Carlo, 2005). Explosive events range from light ash emissions to violent sub-plinian eruptions from the summit craters: the North East Crater (NEC), the South East Crater (SEC), Voragine (VOR) and Bocca Nuova (BN-1 and BN-2) and, since 2011, the New South East Crater (NSEC) (Fig. 1a). During explosive eruptions, a great amount of volcanic particles are injected in the atmosphere. Not only ash-sized particles forming volcanic plumes may be transported over a long distance away from the vent, commonly hundreds of kilometers at Etna, but also lapilli-sized particles and even blocks and bombs can be transported downwind up to several kilometers. Due to prevailing westerly winds, tephra fall deposits are usually dispersed to the East over the Valle del Bove and the eastern flanks of the volcano, sometimes up to Calabria and beyond. The associated tephra fallout may cause damage to buildings, crops and natural vegetation, disruptions of communication and transportation systems, and water contamination (e.g., Blong (1984); Cronin and Sharp (2002); Bebbington et al. (2008); Wardman et al. (2012)) while volcanic ash in the atmosphere is hazardous for aviation because it causes abrasion to surfaces, windshields and landing lights of aircrafts and, in the worst case, ingestion of ash into jet engines may cause their flameout and stalling (e.g., Guffanti et al. (2010)). Among the explosive eruptions of the last century, the 5 January 1990 strong short-lived sub-plinian eruption and the weak long-lived 2002–03 eruption are representative members in terms of duration and thus of potential hazard scenario, because they differ completely in terms of mass eruption rates and column height (e.g., Branca and Del Carlo (2005); Andronico et al. (2008a); Scollo et al. (2013)). In 1990, the SEC produced an eruption column which rose up to 15 km above sea level (a.s.l.) and tephra fallout entirely covered the WNW flank of the volcano. This short event (about 35 min for the climax phase) had a mass eruption rate of ca. 7×10^6 kg s^{-1} in average and a total erupted mass of 1.5×10^{10} kg (Scollo et al., 2013). Instead, a lower eruption column (maximum column height of 7 km a.s.l.) was produced from a 1-km-long fissure between 2850 m and 2600 m on the south flank in 2002–03 and was continuously present for almost two months. For this long-lasting event, the mass eruption rate of the explosive phase was very variable, mostly in the range

Fig. 1. (a) Map of the summit craters; the white lines indicate the crater rim (image courtesy of the cartography laboratory of INGV-OE): North East Crater (NEC), Voragine (VOR), Bocca Nuova (BN-1 and BN-2), South East Crater (SEC), New South East Crater (NSEC) grown on SEC's eastern flank since 2011. The location of the initial pit crater in 2009 is represented with a red dot. (b) Map of radar beam projection on satellite views of Etna's summit area (Google Earth image 23/07/2010). (c) Zoomed map of (b). The range gates over the summit craters are indicated, along with the beam main lobe extension at −3 dB (i.e., 50% of the power received in the beam axis, defining the beam half-aperture: 4.65° in azimuth), at −10 dB (10% of beam axis power), and at −20 dB (1% of beam axis power). (For interpretation of the references to color in this figure legend, the reader is referred to the web version of this article.)

$2– 5 \times 10^4$ kg s^{-1} during its most intense phase, and the total erupted mass was estimated to $4.6 \pm 0.6 \times 10^{10}$ kg (Andronico et al., 2008a). During this eruption, volcanic ash was dispersed in atmosphere, impacting the local economy and causing health problems (e.g., Barnard (2004)). However, even lower intensity events as those that occurred in 2006 and in 2007 (e.g., Andronico et al. (2009), (2008b)), may represent an important risk for aviation and need to be taken into account. More recently, Etna produced cycles of eruptive episodes of the NSEC often culminating in paroxysms with lava fountains feeding ash and lapilli plumes several kilometers high: 25 eruptive episodes between January 2011 and April 2012 (e.g., Behncke et al. (2014)), 13 between February and April 2013, then 8 between October and December 2013 (Andronico et al., 2014).

1.2. Real-time monitoring and forecasting at present

Guffanti et al. (2009) reported seven documented incidents between 1979 and 2006 at the Fontanarossa International Airport in Catania (30 km far from the Etna summit craters), which is considered among the most vulnerable airports worldwide. Ash fallout, in fact, affects airport structures, forcing airport closures, and inconvenience to the Sicilian population and tourism, which all lead to significant economic losses. An efficient monitoring and forecasting system is necessary to give reliable warning and drastically reduce risks during Etna events. For this reason, since 2006 INGV-OE extended Etna's permanent monitoring system to the ash cloud detection mainly through both the installation of new instruments (radar, lidar, disdrometers, thermal and HD cameras, etc.) and the enhancing of the volcanic tremor analysis (Alparone et al., 2007). A dedicated software produces an alert when the seismic RMS changes rapidly and exceeds a fixed value (STA/LTA trigger algorithm); furthermore, the visible and thermal cameras provide images of volcanic activity and the INGV-OE staff on duty 24/7 at the monitoring room sends information to civil protection authorities. The system was later improved to include real-time data from different remote sensing instruments and automatically generated hazard maps that forecast the dispersal and deposition of volcanic ash for different eruptive scenarios (Scollo et al., 2009).

1.3. Need for a complementary radar system

To date, an extensive suite of satellite sensors on various platforms is used for volcanic ash monitoring purposes (e.g., SEVIRI, AVHRR, MODIS), particularly for the (quasi real-time) tracking of the plume extension. Distal plume characteristics can also be retrieved (height, particle diameters, concentrations) based on certain assumptions and conditions. Those systems may suffer limitations due to their restricted temporal (e.g., two images per day for MODIS) or spatial (several km pixels for SEVIRI) coverage. Discrepancy between ground deposits and satellite measurements (e.g., Stevenson et al. (2015)) may also exist, and in some cases satellites cannot detect volcanic ash (e.g., the presence of hydrometeors and ice; for a review, see Prata et al. (2001)). For these reasons, a promising monitoring strategy is the synergetic combination of satellite based sensors with complementary groundbased remote sensing and geophysical sensors. This can potentially provide additional real-time information on explosive or effusive activity (e.g., Gouhier et al. (2012)), including validated eruptive source parameters, as well as on changes in the plumbing system and shallow magma column. There is a particular lack for real-time retrieval of eruption source parameters like particle size distribution, mass eruption rate and total mass. Weather or ad-hoc ground-based radars have

demonstrated their capacity to monitor ash plumes and, consequently, hold the potential to fill this gap and lead to the retrieval of near-source eruptive parameters (e.g., Valade and Donnadieu (2011); Vulpiani et al. (2011); Donnadieu (2012); Gouhier et al. (2012); Valade et al. (2012); Scharff et al. (2012); Marzano et al. (2013)). To this aim, the Italian Civil Protection operates a polarimetric X-band radar in Catania, 35 km south of Etna's summit, able to image the whole plume with a scanning frequency of 10 min and a range resolution of 200 m (Vulpiani et al., 2011; Marzano et al., 2013).

Although long-range powerful fixed weather radar can be used to track ash plumes, short-range compact ground-based Doppler radars are better suited to probe volcanic jets and plumes near the vent at high rate (up to 25 Hz for VOLDORAD; for a review, see Donnadieu (2012)). In particular, while sounding volumes above the vent, they are able to provide all-weather early detection of explosive activity. Continuous measurements of along-beam velocities, directly linked to particle ejection velocities, and of power backscattered by particles, a proxy for the amount of material emitted at the source, bring powerful insights into the column dynamics close to the source (Dubosclard et al., 1999, 2004; Donnadieu, 2012, and references therein; Valade et al., 2012). Furthermore, estimates of tephra mass and mass eruption rate can be recovered through radar power inversion using Mie scattering theory (Gouhier and Donnadieu, 2008; Valade and Donnadieu, 2011). Under certain hypotheses, estimates of gas mass fluxes and total mass may further be retrieved (Gouhier and Donnadieu, 2011).

As a first step toward a quantified monitoring of tephra emissions in near real-time, a ground-based Doppler radar (VOLDORAD 2B) has been installed permanently in a multi-sensor shelter at La Montagnola (2610 m a.s.l.), a peak about 3 km south of Etna's SEC, in July 2009. All-weather remote sensing systems such as VOLDORAD 2B can potentially complement the monitoring and forecasting system developed at INGV-OE (Scollo et al., 2009) by feeding

the institution that is in charge of the surveillance of Etna. One particular goal is to provide accurate and fast information on the evolution of the volcanic plumes during explosive eruptions of Etna. In the framework of the project "Sviluppo ed applicazione di tecniche di telerilevamento per il monitoraggio dei vulcani attivi italiani" granted by Italian Civil Protection and managed by INGV, the Observatoire de Physique du Globe de Clermont-Ferrand (OPGC), France, developed a volcano Doppler radar at 1.274 GHz, called VOLDORAD 2B, to monitor the tephra emissions of Etna's summit craters. Although the VOLDORAD 2B radar is owned by the OPGC, the radar data acquired on Etna are shared between INGV-OE and OPGC in the frame of a collaborative research agreement. As part of the same project, a dedicated micro-patch array antenna, well suited for longterm monitoring in harsh conditions in altitude, was also designed and built at the University of Calabria (Boccia et al., 2010) for INGVOE. In this paper we first describe the radar system, data acquisition and processing, and type of retrieved parameters and their integration within the existing monitoring system of INGV-OE. Furthermore, we document records of volcanic ash plumes detected by VOLDORAD 2B during the activity of Etna summit craters in 2010 and the first of the recent series of lava fountaining events, on 12 January 2011. Their characteristics are analyzed in relation to the observed phenomenology and the instrument limitations. We also discuss advantages of real-time reception of quantified all-weather information on explosive activity during volcanic emergencies, and the future possibilities of real-time radar data integration and assimilation for risk mitigation purposes.

2. Radar system description

2.1. The VOLDORAD 2B radar system

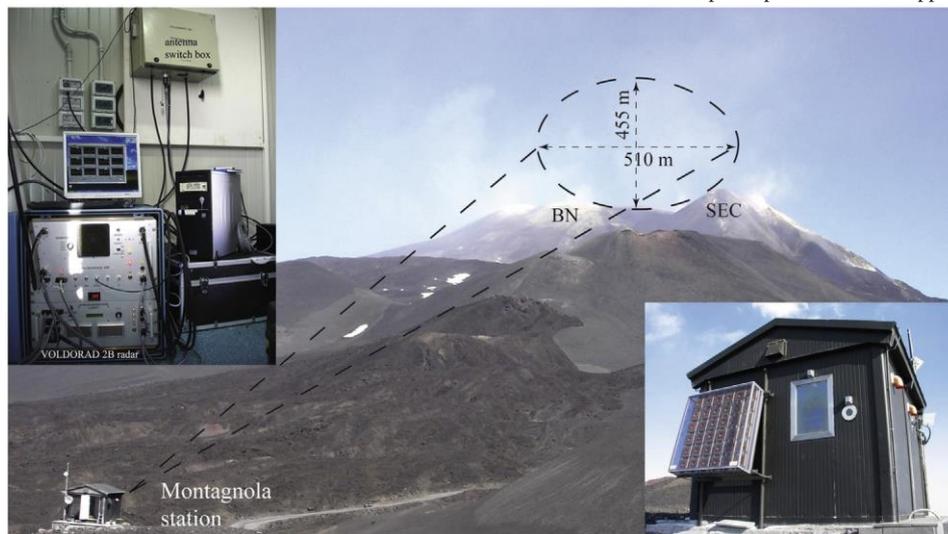The OPGC developed a pulse volcano Doppler radar, VOLDORAD-2B,

Fig. 2. Perspective view of the VOLDORAD 2B radar system (left inset) in the La Montagnola shelter (right inset), about 3.1 km south of the SE Crater (photo F. Donnadieu, July 2009).

dispersal models with eruptive parameters inferred from data measured in real-time. Furthermore, more precise warning can be delivered to the Italian Civil Protection, the national service for the emergency management in Italy, and to aviation authorities such as national MWO (Meteorological Watch Office), Rome ACC (Area Control Centre) and Toulouse VAAC (Volcanic Ash Advisor Centre) to assist the work of air traffic control and enhance the aviation safety.

1.4. Context of VOLDORAD 2B project at Etna

Actions for reducing the hazard from tephra fall were undertaken within the framework of the FIRB project "Sviluppo Nuove Tecnologie per la Protezione e Difesa del Territorio dai Rischi Naturali" funded by the Italian Ministry of University and Research. The project was managed by INGV-OE,

aimed at monitoring Etna's active summit craters. It is based on the previous VOLDORAD-2 system used to investigate the dynamics of Strombolian to lava fountaining activity (Gouhier and Donnadieu, 2010; Donnadieu, 2012, and references therein; Chevalier and Donnadieu, 2015) and ash and lapilli plumes (Donnadieu et al., 2005, 2011; Mora et al., 2009; Valade and Donnadieu, 2011; Donnadieu, 2012; Valade et al., 2012) at several volcanoes like Etna (Italy), Stromboli (Italy), Yasur (Vanuatu), Arenal (Costa Rica), Popocatépetl (Mexico). These radars are derived from a more cumbersome prototype first implemented successfully at Etna in 1998 (VOLDORAD-1; Dubosclard et al., 1999). A technical description of the VOLDORAD-2 radar system is detailed in Donnadieu (2012) and references therein. In the following, only the main properties and modifications of the system proper to VOLDORAD-2B are described. The main characteristics and settings of

VOLDORAD-2B at Etna (Fig. 2) are summarized in Table 1. A new acquisition system was developed by the OPGC using a FieldProgrammable Gate Array chip and LabVIEW control programs in Windows XP environment to provide fast PC-radar communications, a friendly user interface for parameter settings and network communication facilities, while ensuring long-term data and material integrity. The system is controlled remotely through Ethernet connection and the acquisition window can be viewed remotely in real-time. Acquisition can be restarted remotely with modified settings, including three different levels of attenuation (10 dB increment set among five by hardware connections) that can be modified during acquisition. Although the regulated electric supply can be maintained for a few minutes by a battery backup, the system is able to restart automatically after longer power interruption, as sometimes occurs following thunderstorms.

A dedicated vertically-polarized antenna was designed at the University of Calabria, compound of a 6 × 6 array of shorted rectangular patch antennas (Boccia et al., 2010). This provides a directivity and mitigation of grating lobe effects suitable for the radar surveillance of the summit craters without scanning when the radar was implemented. The beam apertures (at −3 dB) of the micropatch antenna are 8.3° in elevation and 9.3° in azimuth as measured from the radiation patterns in the E- and H-planes (Fig. 3). The antenna is fixed to the northern wall of the La Montagnola shelter facing the active craters and is protected from the harsh weather conditions by a flat radome. A new support, allowing some rotation of the antenna, was developed by INGV-OE and is operational since 2012. The implementation of a remote control system for the antenna is considered for the future.

Table 1
Characteristics and main settings of the VOLDORAD 2B radar at Etna.

Parameter (symbol, units)	Value [Selectable range]
Transmitted Frequency (f_t, Hz)	1.274×10^9
Wavelength (λ, m)	0.235
Bandwidth (Hz)	10^6
Power emission at radar output (W)	60
Power transmitted at antenna (P_t, W)	34
Pulse repetition frequency (PRF, Hz)	10^4 [0.5×10^4, 10^4, 2×10^4]
Pulse duration (τ, sec)	10^{-6} [0.4–1.5×10^{-6}]
Radial resolution of range bins (m)	150 [60–225]
Desensitization time from emission (sec)	8×10^{-6} [0–8×10^{-6}]
Patch antenna beam aperture in azimuth at −3 dB (θ_{azim}, °)	9.3
Patch antenna beam aperture in elevation at −3 dB (θ_{elev}, °)	8.3
Number of recorded range bins	11 [1–56] (before 17/12/2013)
	13 [1–56] (after 17/12/2013)
Distance of first and last gates from radar (m)	3135–4635 (before 17/12/2013)
	2685–4485 (after 17/12/2013)
Number of coherent integrations (time domain)	6 [≥1]
Number of incoherent integrations (frequency domain)	3 [≥1]
Number of points used for FFT	64 [64, 128]
Radial velocity resolution (m/s)	3.1 [b36.8]
Maximum radial velocity (m/s)	98.1 [≤1177]
Spectra acquisition interval	0.228 [≥0.05]
Sensitivity (dBZ at 1 km)	~0
Space memory consumption (Go/day)	1.02
Electric consumption (W)	~300
AC power input (V, at 50–60 Hz)	220–240

2.1.1. Measurement principle

Radar is an active remote sensing technique consisting of the transmission of electromagnetic waves (pulsed in the case of VOLDORAD 2B) through a directive antenna focusing most of the energy in a beam (main lobe of the radiation pattern). As they propagate away from the radar, the electromagnetic waves backscatter some energy when encountering reflective targets crossing the beam such as volcanic particles. The received signal is sampled at time intervals corresponding to different distances traveled by the wave, so that information

can be retrieved from different distances, i.e. successively sensed volumes (range gates or bins) along the beam. A Fast Fourier Transform analysis provides the spectral content (amplitude, frequency) of the signal. Frequency shifts (between received and transmitted signals) measured via the Doppler effect are related to radial velocities of moving targets. In addition the contributions of objects with a motion component toward or away from the antenna can be discriminated, respectively as 'negative' and 'positive' radial velocities. Interpretations of these contributions may differ depending on the type of activity (e.g., Dubosclard et al. (2004); Donnadieu (2012)). Thus, the basic information, namely Doppler spectrum, displays the power distribution (i.e. power spectral density) across velocity classes, for each volume at each time step.

2.1.2. Radar retrievals

Two main types of information are retrieved from Doppler spectra for each probed volume: (i) along-beam (radial) velocities, in particular maximum radial velocities (N0 and b0); (ii) power backscattered by particles. Since the backscattered power is dominated by reflections from particles, it is a proxy for the quantity of tephra crossing the beam. More on the scattering theory and echoing mechanisms by volcanic particles can be found in Dubosclard et al. (1999), (2004); Gouhier and Donnadieu (2008) and Donnadieu (2012). The latter also points out the importance of the tephra sizes relative to the wavelength in the interpretation and modeling of radar echoes. Operating in the Lband (λ = 23.5 cm), VOLDORAD-2B allows the detection of explosive activity under any weather conditions, without much attenuation by hydrometeors, by sounding the interior of even dense particle-laden plumes.

2.1.3. Sounding conditions at Etna

The radar beam axis initially pointed northward (N347.5°) to the summit craters from La Montagnola with an elevation angle of ~15.5° (Figs. 1 and 2). The beam aperture at −3 dB is 8.3° in elevation and 9.3° in azimuth, corresponding respectively to 455 m and 510 m at 3135 m. Eleven volumes, 150 m deep were probed from 3135 to 4635 m, hence covering the entire summit area (Table 2). Due to the Eastward migration of activity at NSEC, the antenna pointing was adjusted to azimuth N355.2° and elevation +14.9° on 10 October 2012. Two additional gates at 2685 m and 2835 m are also recorded since 16 December 2013, in order to better capture fallout from the NSEC in cases when they are blown southward by the wind.

Table 2
Radar range gates characteristics.

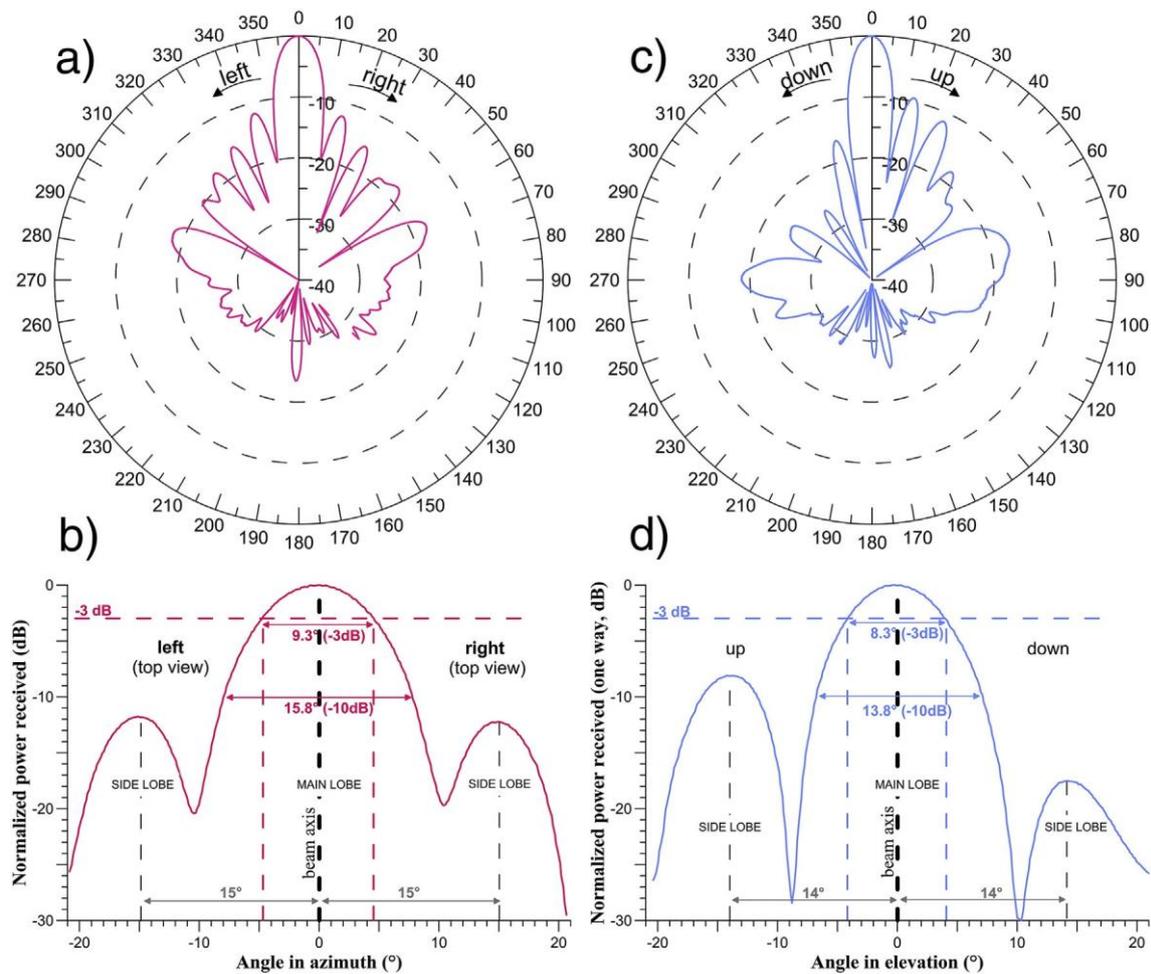| Gate range from radar (m) [2009–2013]	Volume at −3 dB ($10^6 m^3$)	Vertical dimension (m) at −3 dB (8.3°)	Horizontal dimension (m) at −3 dB (9.3°)	Crater
3135	27.2	455	510	SEC/NSEC
3285	29.9	477	534	SEC/NSEC
3435	32.7	498	559	
3585	35.6	520	583	
3735	38.6	542	608	BN/VOR
3885	41.8	564	632	BN/VOR
4035	45.1	586	656	
4185	48.5	607	681	NEC
4335	52.1	629	705	NEC
4485	55.7	651	730	
4635	59.5	673	754	

Fig. 3. Radiation patterns of the micro-patch antenna array in the H-plane (azimuth; a and b) and E-plane (elevation, c and d) (OPGC note 20121132).

2.2. Radar data acquisition on Etna

2.2.1. Data format and transmission

The data acquisition software allows the recording of the raw signal or the power spectra of each gate, or both. Only Doppler spectra are recorded at Etna, being directly computed from the raw time series (6 coherent integrations) and then averaged in the frequency domain (3 incoherent integrations). These settings (Table 1) turn out to be a good compromise between data storage and transfer rate (1 GB/day) at relatively high acquisition rate of 4.4 s⁻¹ (0.228 s). The power spectral density, i.e., power values of the 64 velocity classes, is recorded for each gate at each time step and stored in 1 min-long, time-labeled binary files. The clock of the acquisition PC, used to time-reference the radar data, is synchronized every hour to Coordinated Universal Time (UTC) time by the local server, allowing precise comparison with other timereferenced data recorded by the INGV-OE instrumental network. Once completed, the data file is copied into a server in the La Montagnola shelter and then transmitted to INGV-OE in Catania using a wireless connection link (5 GHz — distance about 30 km). Then, they are stored on a data server and duplicated to OPGC server within two minutes. In order to optimize the data storage (1 GB/day), a dedicated lossy compression algorithm was developed to reduce the size of the data up to 5 times. The introduced error during the compression is 2% with respect to the internal noise of the radar, not affecting the data content. At INGV-OE, the data are then processed in real-time to reveal any volcanic activity and finally stored.

2.2.2. Real-time products and radar database

Upon reception at INGV-OE, the radar data are debiased and filtered with respect to the time and subsampled to get 5 spectra per minute. Following a method similar to Valade et al. (2012), a radar-derived detection index is computed from the radar-derived parameters in order to best identify tephra produced by the explosive activity. The temporal evolution of this index is displayed in real-time in the INGV-OE monitoring room and used to trigger automatic alert messages. The radar index is obtained as follows: (i) ground echoes in the Doppler spectra (around the zero velocity) were sampled at various moments and averaged, taking advantage of their remarkable stability through time; (ii) this average is then used to filter ground echoes out of Doppler spectra stacked over a large number of successive samples; (iii) the stacked filtered Doppler spectrum is integrated over the full velocity spectrum providing a power-based time series.

These filtered data are integrated in order to obtain the power echo of the signal for each gate. The values are also stored inside the multidisciplinary database of INGV-OE in order to allow a real-time consultation and visualization in the monitoring room. The resulting time series allows unambiguously detecting lava fountains feeding ash and lapilli plumes.

A simple automatic system was implemented for early warning at the onset of a tephra emission from Etna's summit craters. A double threshold method is used to release automatic alert messages minimizing false alarms. Whenever the radar signal increases above the first threshold and keeps increasing for more than 5 min (second higher threshold), the system alerts the operators in the monitoring room with a sound and sends an e-mail to a predefined mailing list to notify of the start and the end of the explosive event. The onset and end times of the paroxysmal phase featuring a sustained eruption column are picked accurately

in most cases, with the exception of slowly emergent and waning signals. During the series of lava fountaining episodes of the NSEC, the index was based on the 3285 m range gate, which roughly corresponds to the distance from the radar to this crater. The alert system was tested during the volcanic activity of the Etna from January 2011 to November 2015. In this way, very few false alarms occurred, being mainly due to storms while 46 eruptive episodes were detected correctly. The only two failed detections were due to electricity blackouts and the subsequent breakdown of the acquisition software. The system is therefore quite robust even in adverse weather conditions in altitude.

In addition to the use of real-time radar signals by INGV-OE for the volcanic monitoring of Etna, raw Doppler spectra are displayed in near real-time every minute on the OPGC VOLDORAD website and time series of the echo power from different distances are shown in real-time for an early discrimination of the active crater. An open database of radar products computed from the raw data is made available from the VOLDORAD service on the OPGC website: http://voldorad.opgc.fr/ (Donnadieu et al., 2015). Upon a user's request, up to 9 parameters are automatically computed for each gate from the raw data files (e.g., Dubosclard et al. (2004)) and released into a table which can be downloaded.

2.2.3. Post-processing radar retrievals

The power backscattered in each sampled volume (range 'gate' or 'bin') is computed by summing the power for all the velocity classes (Dubosclard et al., 2004). The power received by the radar was calibrated for individual Doppler frequencies (hence radial velocities) with a frequency generator, so that retrieved echoes can be used to quantify the tephra mass in the beam using an electromagnetic model (Gouhier and Donnadieu, 2008), provided that the particle size distribution is constrained. The measured maximum radial velocity (on either side of the spectrum, positive and negative) is defined as the highest velocity class for which power is superior to the power noise level. With the settings chosen at Etna (Table 1), the maximum radial velocity measurable without aliasing is 98.1 m/s, and the radial velocity resolution is 3.1 m/s.

3. Examples of radar signals induced by ash plumes

In the following paragraphs we illustrate some examples of radar signals recorded during Etna's explosive activity ranging from ash emissions from a new pit on the lower slope of the SE cone and from Bocca Nuova to sustained lava fountaining from the New SE Crater.

3.1. Detection of short-lived ash plumes

3.1.1. The 8 April 2010 ash plume

Although its 23.5 cm wavelength is not optimal to detect volcanic ash, VOLDORAD 2B recorded several eruptive phenomena from Etna's summit craters, including short-lived ash emissions. A few months after the radar installation on La Montagnola (July 2009), a new pit crater opened on 6 November 2009 at ca. 3100 m a.s.l., on the eastern flank of the SE crater. In the first months of 2010, the pit crater emitted discontinuous whitish plumes accompanied by profound rumbling. The first significant ash plume after its formation occurred on 8 April 2010, when a small eruption column rose up to ≤1 km above the crater rim starting around 16:28 UTC (Andronico et al., 2013). It lasted for about 10 min although the emission of ash was limited to a few minutes only and ended with water vapor mostly (Fig. 4). The column was initially vertical, grew up to about 600–700 m in height and 200 m in width within 40 s, but was soon bent by the winds. After 16:34 UTC, the plume became whitish, indicating cessation of ash emission and mainly degassing ongoing. Volcanic ash and small lapilli were dispersed NE by winds during 10 min (Corsaro, 2010; Andronico et al., 2013). INGV Videos of the 8 April 2010 event showed that the ash plume formed from the new pit crater on the eastern flank of the SE cone. Despite the location of the vent lower and offset by about 1° from the conical beam pointing at the summit craters, thus outside the 4.6° halfaperture, VOLDORAD was able to detect echoes from the ash column in the 3285 m range gate, with an unambiguous eruptive signal for about 10 s starting at 16:28′25

UTC. During the detection sequence the along-beam component of the velocity measured by the radar inside the plume at the beam elevation ranged from 15 to 25 m/s, consistent with the plume front ascent velocity of about 17 m/s inferred from INGV-OE videos. In the case of mainly convective ash plumes, maximum radial velocities are thought to represent directly the maximum speeds of particles convecting inside the plume eddies probed by the radar, unlike for lava jets where a geometrical conversion must be applied to retrieve upward velocities (Donnadieu, 2012). This suggests a relatively weak or/and short-lived momentum at the source and a plume ascent mechanism quickly dominated by buoyancy. Echoes likely stem mainly from the westernmost enlarged top part of the plume (mushroom) expanding upwind inside the −3 dB limit of the main beam lobe (Fig. 5). Due to the decreasing radiation pattern of the main lobe sideways (from 50% at 4.6° of the beam axis to 1% at 10°; Figs. 1, 3), the contribution to the detectable eruptive echo of the plume's main body (offset to the East) was likely minor. The echo contribution of particles associated with a northward velocity component (P+ 3285 m) is higher, certainly resulting from the wind speed component in this direction. As a matter of fact the detectable eruptive signal lasted mainly 10 s (although it can be followed for another 7–8 s) and remained weak (only 3 dBm above the background noise), suggesting a small size of emitted particles. Indeed, Andronico et al. (2013) found 90% of particles with dimensions ranging from 0.125 to 1 mm showing a modal value of 0.25 mm. One sample had a slightly broader trend with a secondary mode peaked at 8 mm, which is attributed to a different pulse of ash emission. Given the early detection by the radar (16:28:25 UTC), we interpret the small lapilli to have been present mainly in the initial mushroom and to have caused the radar signal to exceed the detection threshold despite the fact that the plume filled only a fraction of the probed volume. It is likely that mainly infra-millimetric particles were emitted during the following minutes, and then followed by steaming. The offset of the ash column to the East with respect to the beam axis and the NE bending forced by the winds both explain that the rest of the emission remained undetected.
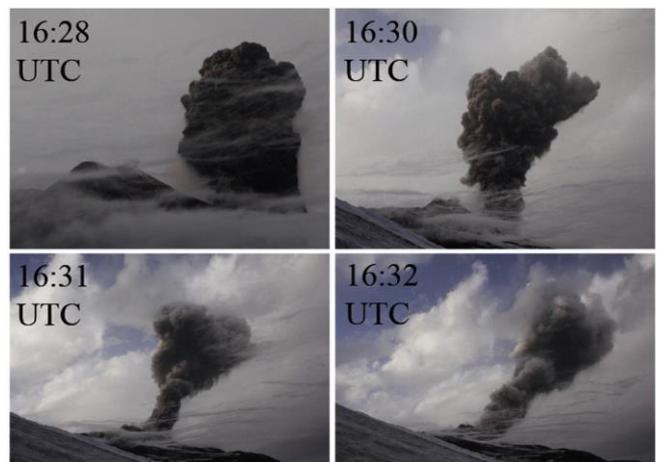

Fig. 4. Tephra plume emission on 8 April 2010 at 16:28, 16:30, 16:31, 16:32 UTC. Photos from http://www.flickr.com/photos/bretscher/sets/72157623824783982.
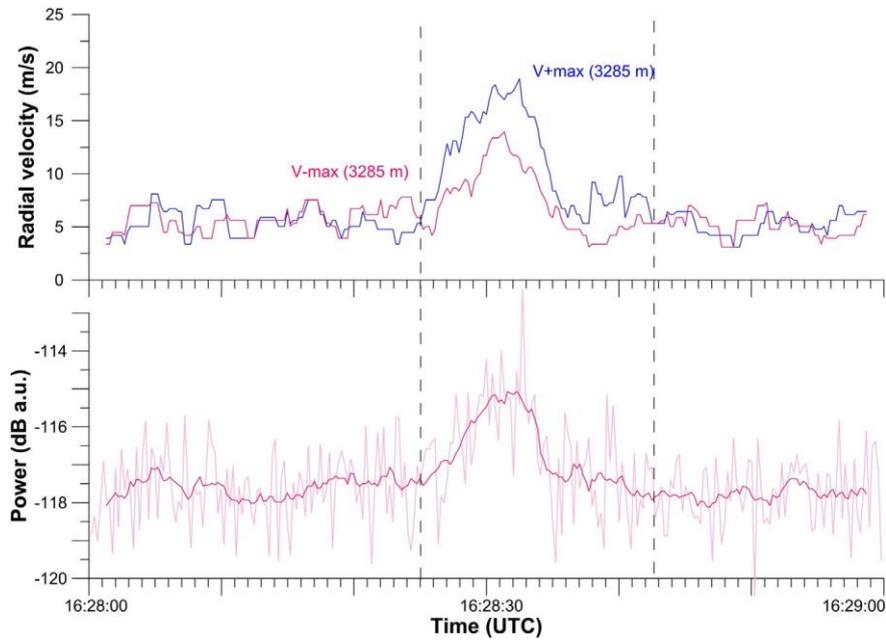
Fig. 5. VOLDORAD 2B records of the 8 April 2010 ash plume from the new pit crater on eastern flank of Etna's SE Crater. The radar time series show echo power and maximum radial velocities measured in the 3285 m range gate (see Fig. 1c).

3.1.2. The 25 August 2010 ash plume

On 25 August 2010, the Bocca Nuova 1 (westernmost pit) crater produced a light ash emission. The event, registered by INGV-OE videosurveillance system began at 13:09 UTC and lasted about a dozen of minutes (Fig. 6). The eruption column was entrained to the SE by winds and finally rose up to N1 km above the crater rim. Fallout, mainly composed by fine particles (Lo Castro, 2010), poured over the southeast flank of the volcano reaching Catania (INGV — Rep. N° 35/2010). The plume reached over 1 km in height within 1 min, indicating a mean ascent rate of 17 m/s for the plume front, and 22 m/s during the first 10 s (Andronico et al., 2013).

In the radar record, the ash emission can be tracked in mainly two range gates at 3735 m and 3835 m (Fig. 7), identifying Bocca Nuova as the source of emission (Donnadieu, 2012; Table 2) and constraining the plume width to less than 300 m in the N–S direction. The ash plume is detected around 13:09′10 UTC, filling both sounded volumes at the same rate for a few seconds, with internal velocities of 18– 22 m s^{-1} measured at the beam elevation. Soon, most of the reflective tephra are taken out of the 3885 m range gate by winds toward SSE, whereas the 3735 m range gate progressively fills up until 13:09′20″, when the tephra flux out of the sounded volume starts to exceed the flux in. The majority of the tephra filling is constantly being pushed southward by the wind as attested by the
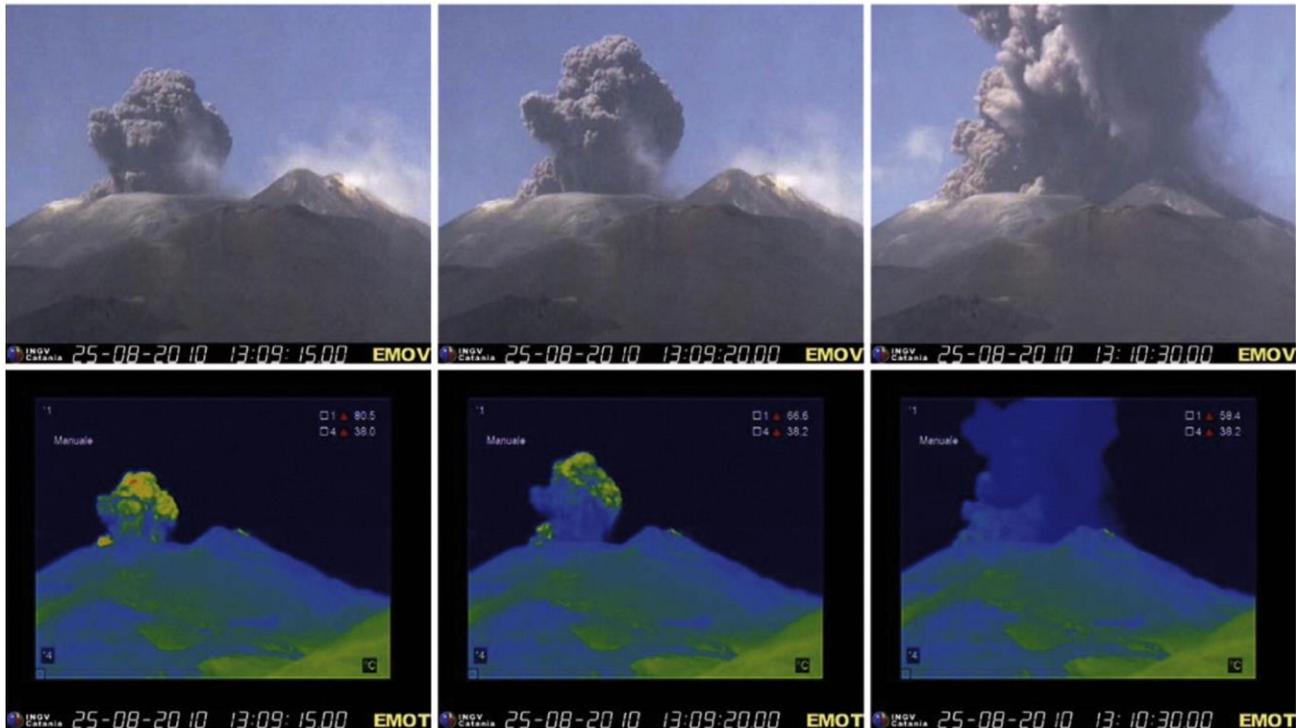

Fig. 6. Tephra emission of 25 August 2010 from Bocca Nuova crater of Etna viewed by INGV-OE EMOV (visible, top panels) and EMOT (thermal, bottom panels) cameras at the Montagnola station.

overwhelming power associated with southward radial velocities (Fig. 8). The eruptive signal shifts toward negative radial velocities in a matter of seconds attesting the southward wind advection. The mode of the power distribution ends up at 5–10 m s^{-1}, which represents the southward component of speed of the majority of ash particles. The spectral width of the eruptive signal (~25 m s^{-1}) indicates particle convective motion during advection by the wind. The stronger upward momentum in the first seconds is responsible for the larger spectral width (Fig. 8 top panel) and induces echoes with positive velocities, also in the upwind gate at 3885 m. In total the detected eruptive signal lasts about 30 s with the most significant amplitudes occurring within the first 20 s. However, videos in the visible band show weak emission of fine ash going on for several minutes. Also the infrared images (7.5–13 μm, 320 × 240 pixels, IFOV 1.3 mrad, 6.1 m/pixel at distance of NSEC) from the ground-based FLIR A40M thermal camera at La Montagnola indicate above-background apparent temperatures starting at 13:09:01, peaking at 169 °C after 3 s and decreasing progressively (Fig. 7). The infrared signal, tracking the plume immediately above the crater rim, is ahead of the radar echoes by 10 s because radar detection occurs only after the plume (200 m high) has reached the beam margin and a significant fraction of it has entered into the beam. Importantly, both the radar and the infrared signals have the same duration. Considering that the main heat reservoir is compound of particles rather than gas and that the radar signal is mainly sensitive to particle concentration and sizes, this suggests that the initial mushroom forming the top-most portion of these discrete ash plumes is either bearing larger particles in average or more concentrated, or both, than the ensuing tail (or root) having less concentrated and/ or finer ash particles that remain undetected at the radar wavelength. This seems to be a common feature to many other discrete short-lived ash plumes of Etna. It might be explained by an initial clearing of particles obstructing the vent before finer ash (mainly remobilized material in most cases) can be entrained by the expanding gas.

Other eruptive radar signals were recorded during short-lived ash emissions from Bocca Nuova crater on 22 October (16:23 UTC, >60 s) and 22 December 2010 (04:46 UTC, >30 s) despite strong winds preventing the ash plume uprise.

These examples show that, by sounding the atmosphere just above the summit craters, near the emission source, short-lived emissions ash and small lapilli can be detected by VOLDORAD 2B at Etna despite its non optimal wavelength. They also suggest that the initial emission of a discrete ash plume, including the developing front, likely contains the largest particle sizes (coarse ash and possible small lapilli) and concentrations at least within the first hundred meters. For these shortlived ash plumes, the highest particle mass flux seems to occur typically within the first 10 s, decreasing thereafter (along with particle sizes), not allowing for a high eruption column to be sustained.
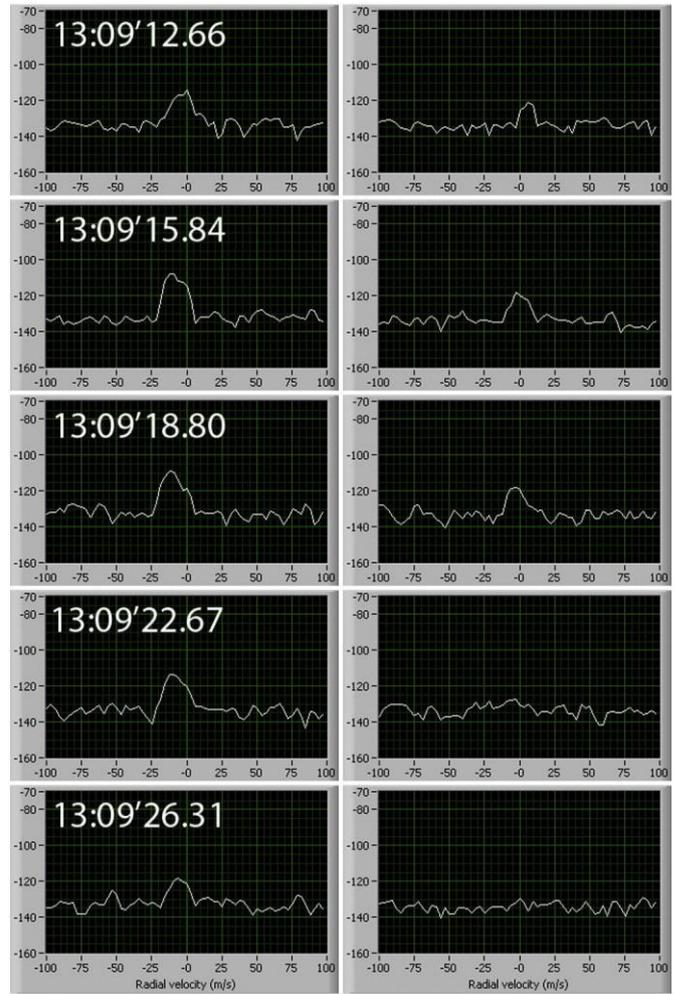

Fig. 8. Doppler spectra recorded by the radar in the 3735 m (left panels) and 3885 m (right panels) range gates during the short-lived ash plumes emitted by Bocca Nuova crater on 25 August 2010 (times in UTC). They show the power spectral distribution versus alongbeam velocity components measured by the radar (negative toward the radar to the south, positive away from it to the North).
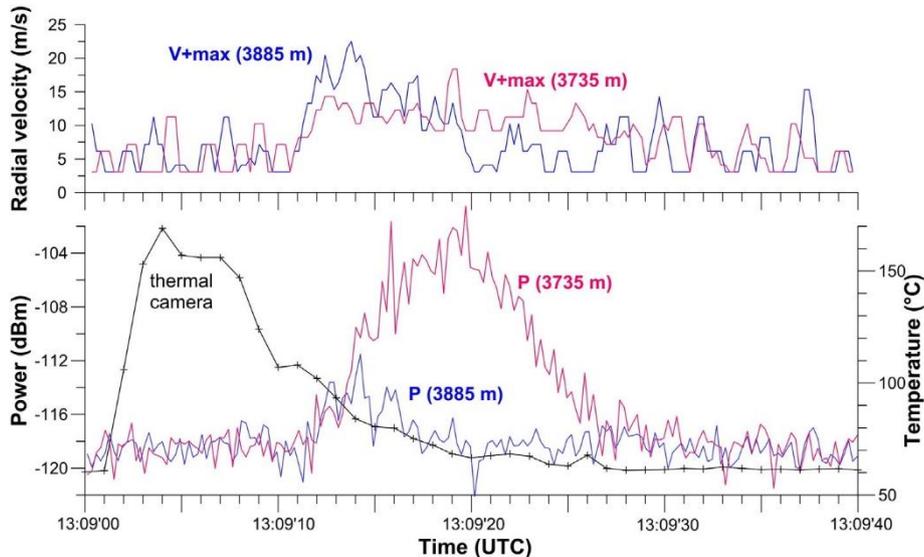

Fig. 7. VOLDORAD 2B records of the 25 August 2010 tephra emission from Bocca Nuova crater BN1. The radar time series show positive maximum radial velocities (top) and echo power (bottom) measured in the 3735 and 3885 m range gates. The maximum apparent temperatures of the FLIR thermal camera at La Montagnola station are plotted.
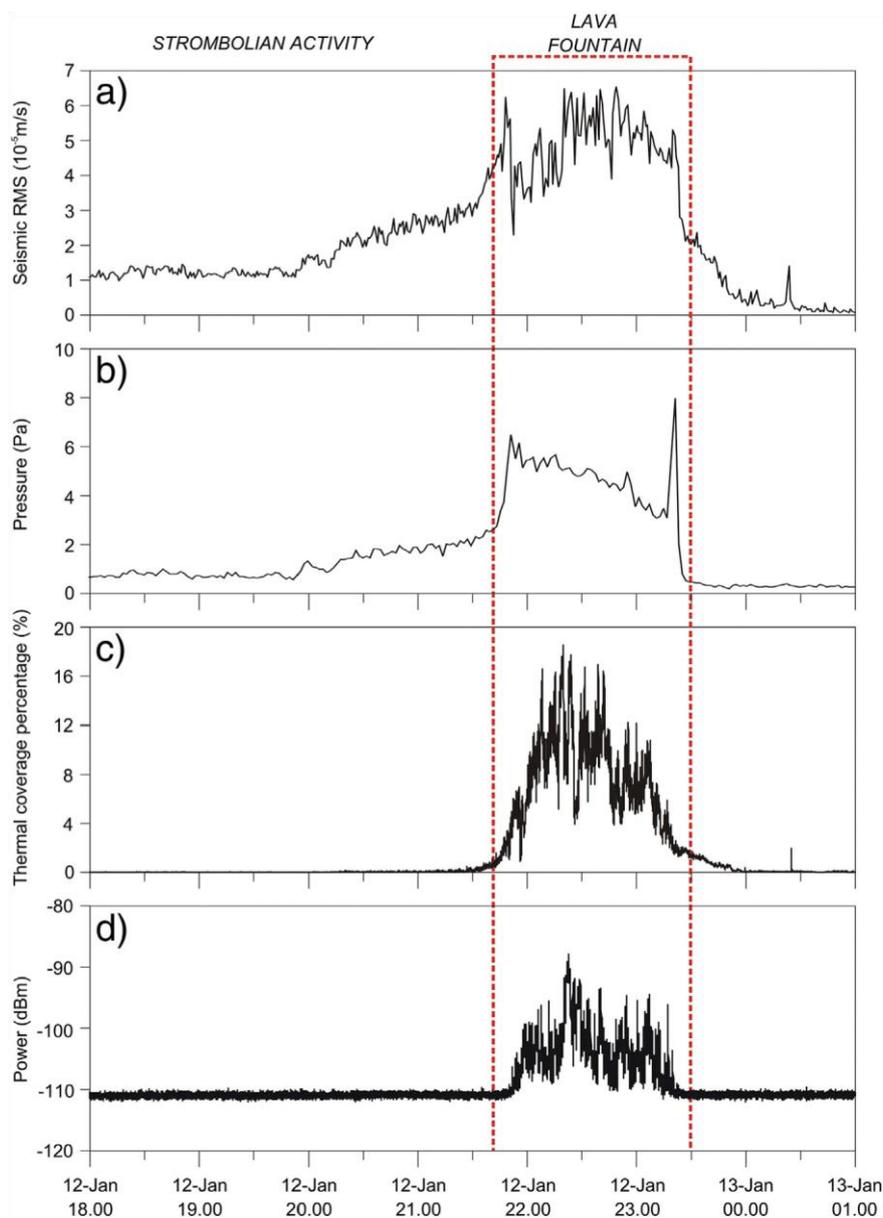
Fig. 9. (a) RMS of the seismic signal recorded at the vertical component of EBEL station and filtered in the frequency band 0.5–5.5 Hz. (b) RMS of the infrasonic pressure recorded at EBEL station and filtered in the frequency band 0.5–5.5 Hz. (c) Percentage of area coverage of the anomaly from EMOT thermal camera. (d) Total echo power backscattered by particles crossing the VOLDORAD 2B radar beam at La Montagnola station.

3.2. Detection of lava fountaining events feeding ash and lapilli plumes

Etna volcano initiated a new cycle of lava fountaining episodes in the night of 12 January 2011, producing spectacular lava fountains and an ash and lapilli plume, originating from the new pit down the east flank of the SE Crater, that later formed a cone and was named the New SE Crater (NSEC). The eruptive episode started on 11 January 2011 with weak Strombolian activity inside the pit crater that intensified on 12 January evening, as attested by the increase of seismic RMS and infrasonic pressure (Fig. 9a, b). The transition to lava fountain between 21:40 and 21:50 UTC was marked by an abrupt increase of seismic, infrasonic, thermal and radar signals (Fig. 9). Lava fountains reached 800 m high and an ash and lapilli column rose above the fountain more than 6 km in height (Calvari et al., 2011; Andronico et al., 2014). The dispersion of fallout toward SSW led to the closure of the international airport of Catania during several hours. Lava flows advanced eastward up to 4 km away from the vent, reaching Valle del Bove. The explosive activity stopped at about 23:55 UTC. Calvari et al. (2011) estimated dense rock volumes of ~0.85 × 10^6 m^3 for the pyroclastics

erupted during the lava fountaining phase. Andronico et al. (2014) inferred a total erupted mass of tephra of $1.5 \pm 0.4 \times 10^8$ kg, with a mass eruption rate of $2.5 \pm 0.7 \times 10^4$ kg s^{-1} during about 100 min. Calvari et al. (2011) estimated a volume of 0.84–1.7×10^6 m^3 for lavas erupted during the effusive phase. The latter value is in agreement with the 1.2×10^6 m^3 found by Gouhier et al. (2012) from satellite data, providing a mean effusive output rate of 55 m^3 s^{-1} over the 6 h of emplacement.

VOLDORAD 2B was able to detect tephra emission mainly in the two range gates closest to the crater (3135 and 3285 m) between 21:40 and 23:40 UTC on 12 January and up to five gates (3135–3735 m) between 22:20 and 22:30 UTC (Fig. 10). As the beam was initially aligned on the summit craters rather than on the NSEC (the antenna was rotated more toward the NSEC on 10 October 2012), the signal is likely dominated by the fallout of ballistic blocks, bombs and coarse lapilli from the lava fountain and by the lateral ejection of tephra rather than by fragmenting lapilli and ash feeding the ash plume rising above the lava fountain. Echo power peaked at −90 dBm between 22:20 and 22:24 UTC during the climax as a result of the lava fountain widening (and/or a temporary orientation of the
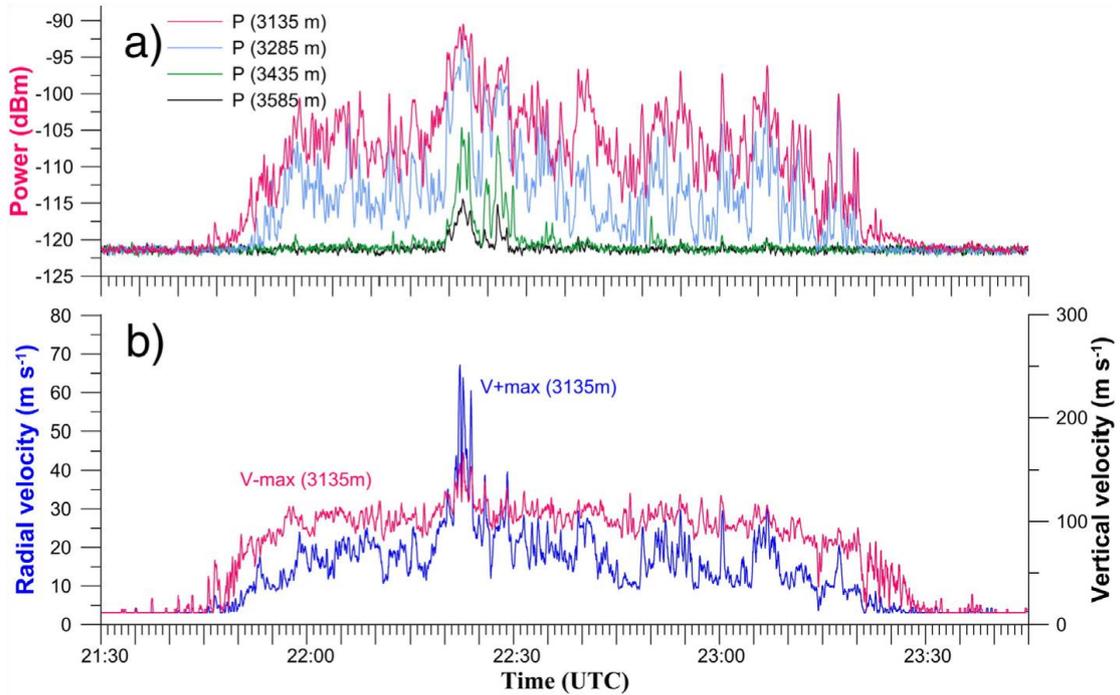
Fig. 10. Radar parameters measured in the main range gates during the 12 January 2011 paroxysmal episode of the New SE Crater initiating the 2011–2013 cycles of lava fountaining events. (a) Backscattered power (12.5 s time and frequency smoothing). (b) Along-beam velocities.

fountain toward the beam caused by the wind) and increase in intensity (Calvari et al., 2011). At this time, vertically ascending particles clearly crossed the radar beam and caused measured radial velocities to strongly increase, commonly exceeding 67 m s⁻¹ with peaks reaching over 80 m s⁻¹ (Fig. 11). These radial velocities during the climax convert to vertical velocities of 250 m s⁻¹, and over 300 m s⁻¹ respectively, by using a geometrical factor of 3.74 inferred from the sounding configuration and assuming chiefly vertical ejection inside the beam during the minutes of climax. Ejection velocities can be used to calculate pyroclastic fluxes, as discussed in Section 4.1. It is unlikely that crosswinds significantly affect upward velocities and corresponding along-beam

components measured inside the lava fountain at the beam bottom but they clearly orientate the fallout and influence the associated along-beam velocity component measured by the radar. The wind advection southward is mostly visible in the gate downwind (3135 m) with strong echoes associated with larger negative velocities (Fig. 12). The pulsating behavior of the lava fountain flux is clearly seen in Figs. 11 and 12, including 20 to 40 s long oscillations of measured echo amplitudes and velocities. Characterizing and understanding this pulsating behavior require a thorough analysis beyond the scope of this article but it likely originates from the dynamics of the magmatic conduit and reservoir.
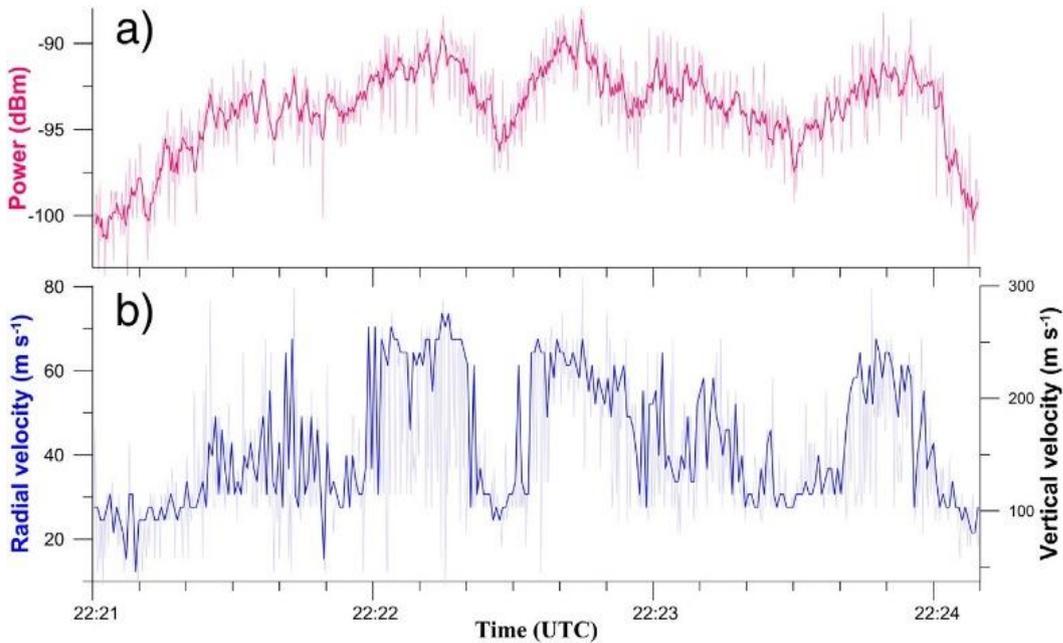

Fig. 11. Radar parameters measured in the 3135 m range gate during the climax of the 12 January 2011 lava fountaining event. (a) Backscattered power: 4.4 Hz raw data and 5 points running average in bold. (b) Positive (northward) along-beam velocities: 4.4 Hz raw data and average over 3 spectra in bold. Inferred vertical velocities are indicated on right scale.
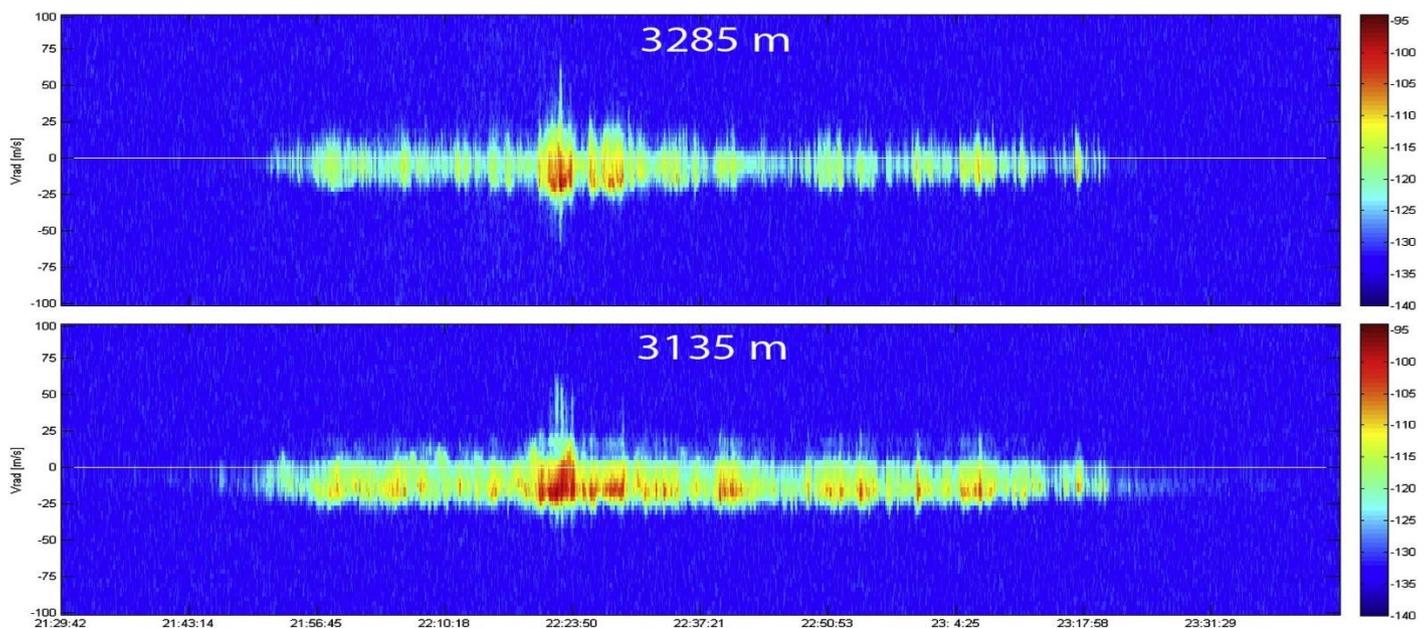
Fig. 12. Radar velocigrams of the 12 January 2011 lava fountain showing the time evolution of power spectral distribution among the Doppler velocities in the two main range gates closest to the New SE Crater vent.

4. Discussion

4.1. Velocimetry and mass loading retrievals

Radar along-beam velocities of 45–90 m s⁻¹ have been measured by VOLDORAD during several other lava fountaining events at Etna such as those on 13 July 2001 at SEC (Donnadieu et al., 2003, 2005), on 23/11/ 2013 at NSEC and on 03/12/2015 at VOR (Donnadieu et al., 2015). Assuming chiefly vertical ejection and no significant block deceleration before entering the beam bottom (100 to 200 m above the vent), values in the range 175–350 m s⁻¹ can be regarded as representative of lapilli and block maximum ejection velocities above the vent during lava fountain paroxysms at Etna. Peak vertical velocities in the range 350– 400 m s⁻¹ have even been inferred from radar measurements closer to the vent during the violent formation of the Laghetto cone at Etna in July 2001 (Donnadieu et al., 2005).

With the technological developments in the recent years, high particle velocities have also been measured in Strombolian lava jets. Using a thermal camera, Harris et al. (2012) report lapilli-sized particles moving vertically near the vent at up to 213 m s⁻¹ at Stromboli during normal activity. Gaudin et al. (2014) found maximum vertical velocities of 160 m s⁻¹ (up to 200 m s⁻¹) for bombs coarser than 10 cm at Stromboli and Yasur volcanoes using a high-speed camera in the visible. Taddeucci et al. (2012) measured at-vent velocities up to 405 m s⁻¹ associated with cm-sized particles entrained by the gas using high-speed highresolution imagery in the visible at Stromboli. Bombrun et al. (2015) measured near-vent velocities of coarse lapilli up to 240 m s⁻¹ using lower resolution high-speed thermal videos. Radar-derived particle velocities of about 250 m s⁻¹ (105 m s⁻¹ measured along-beam with a dip angle of 25°) are reported by Harris et al. (2013) and Chevalier and Donnadieu (2015) at Stromboli.

Ejection velocities can be used to calculate pyroclastic fluxes. Values of 250 m s⁻¹ have been measured by VOLDORAD 2B during the climax of the 12 January 2011 event, when the lava fountain became wide enough to vertically cross the beam. Considering the same parameters used by Calvari et al. (2011), i.e., a vent diameter of 30 m and a proportion of magma in the jet of 0.18% (S. Calvari, pers. comm.), we calculate a dense rock equivalent (DRE) pyroclastic flux of 318 m³ s⁻¹ during the climax (22:20–22:24 UTC), with brief peaks over 380 m³ s⁻¹. This is twice the maximum flux that can be inferred from the

maximum upward velocities of 125 m s⁻¹ found by Calvari et al. (2011) at 22:21 UTC. As the pit crater was off the beam axis, it was only possible to measure upward velocities in the radar beam during the 4 min climax. Therefore, we can only speculate a DRE mean flux of 185 m³ s⁻¹ by using the same relative variations of velocities derived from fountain height observations of Calvari et al. (2011), i.e. twice the mean output rate calculated by these authors. This would lead to 1.3×10^6 m³ of tephra erupted during the 2 h of lava fountaining detected by the radar, neglecting the amount of tephra emitted during the Strombolian phase. Note that the pyroclastic fluxes and total volume were estimated from radar maximum velocities inside the lava fountain. Therefore, although not obtained at the vent but 100–200 m above the vent, these mass loading parameters likely represent upper bounds if values assumed for the vent diameter and the pyroclast fraction in the jet are correct. The much lower total erupted tephra mass found by Andronico et al. (2014) from the tephra plume deposits of the 12 January 2011 event suggests that ash and lapilli transported downwind might represent as little as 5 % of the total mass of tephra erupted during lava fountaining. Our estimates compare well with the 1.6×10^6 m³ DRE volume erupted during all the lava fountaining phase of the most violent event on 23 November 2013, giving a time-averaged-discharged-rate of 360 m³ s⁻¹ (Bonaccorso et al., 2014).

4.2. Expected benefits

The VOLDORAD 2B Doppler radar turns out to be a powerful allweather tool for detection and tracking of tephra emissions through high rate continuous sounding of juxtaposed atmospheric volumes, providing reflectivity and velocity data in the spatio-temporal domain. It allows us to both improve the monitoring of Etna and address quantitatively scientific issues on ash plume dynamics and eruptive behavior in the short- and mid-term. This is particularly valuable in the context of a rapidly evolving system, as occurring nowadays, during the fast reactivation of volcanic activity at Etna's summit craters, such as the formation and growth of the NSEC. Radar retrievals are also complementary with models of plume ascent and ash dispersal to improve hazard assessment and risk mitigation; it is expected, in the nearfuture, that estimates of mass fluxes in quasi real-time (e.g., in the continuation of Gouhier and Donnadieu (2008)) can feed models of tephra dispersal to refine the prediction of ash fallout areas. It is worth noting that, although model input parameters used in the forecasting system at INGV-OE were obtained by a detailed analysis of the past eruptions (e.g., 2001

Etna eruption in Scollo et al. (2007)), the forecasted activity may differ gnificantly from the real eruption. Consequently, outputs of the forecasting model should be considered only as preliminary pictures of volcanic ash dispersal and fallout. From the lesson of the Eyjafjallajökull eruption in Iceland in April–May 2010, it has been well recognized by the scientific community that volcanic ash forecasting may be improved only with detailed knowledge of eruption source parameters (Elbern et al., 2010). In addition, sensitivity analysis and parametric studies on tephra dispersal models have also shown that if values of some input parameters are modified (e.g., the total mass), the results of numerical models may differ greatly (Connor and Connor, 2006; Scollo et al., 2008a, 2008b; Webley et al., 2009). Consequently, their setting should be done with great care in order to make volcanic ash forecast as close as possible to the real dispersal. To reach this aim, inverse modeling and data assimilation represent the future challenge but they need automatic techniques able to combine numerical models with source terms obtained for example by remote sensing system such as VOLDORAD 2B. Another possible outcome is, importantly, the estimation of the mass eruption rate of tephra and its temporal variations, and the total mass of particles emitted. Firstly, tephra mass could be derived from radar power time series by inversion (Gouhier and Donnadieu, 2008). Then, using a simple physical model for the ash plume transit through the radar beam, the mass and velocity time series could be integrated through time to obtain the mass flux evolution and the total mass. Although this requires assumptions on an average particle size (e.g., from analysis of previous similar events), the mass flux of tephra is a key parameter needed for plume monitoring and modeling that can be estimated quantitatively from the radar kinetic and loading parameters (Donnadieu et al., 2005; Gouhier and Donnadieu, 2008, 2011; Valade and Donnadieu, 2011; Donnadieu, 2012).

Besides, such eruptive parameters, inferred from ground-based Doppler radars measurements near the emission source with high temporal resolution (0.2 s for VOLDORAD) and a spatial resolution of tensof-meters, can also complement ash cloud tracking by satellite imagery: (1) to assess the intensity during the first minutes of an eruption when satellite images are not yet available, (2) to compare the mass of tephra injected in the atmosphere with that emitted at the source, (3) to provide information where satellite images cannot be used (e.g., undetected atmospheric ash content, too small ash column, overcast weather, and insufficient rate of image delivery with regard to the ash cloud displacement rate).

4.3. Limitations

VOLDORAD 2B does not allow detection of gas bursts without significant amounts of solid particles, although these do not generate directly a strong threat. Dilute ash plumes are not detected either by the automatic warning algorithm but careful retro-analysis sometimes show weak peaks of the signal to noise amplitude (N3 dB) in the range gate right above the crater, concomitant with discrete emissions or pulsating activity with a low ash content. Such a correlation, clearly at the limit of detection, was found during some sequences of intermittent degassing at NEC on 15 November 2010. The pulsating degassing with low ash content became continuous forming a diluted, thin weak plume bent over northward after rising 100–300 m (Andronico et al., 2013). One sample collected by these authors on the crater rim shows a relatively wide, coarse-grained distribution ranging from 0.063 mm to more than 8 mm, with a mode between 0.25 and 0.5 mm. Using a groundbased lidar on 15 November, Scollo et al. (2012) measured ash concentration greater than 4×10^{-3} g m^{-3}. With this concentration, we infer the main contribution to the radar echoes recorded during this activity to come from lapilli 7–8 mm in diameter. This is consistent with the maximum size of pyroclasts found in proximal deposits by Andronico et al. (2013), despite the fact that more than 80% of the sample ranged from 0.25 to 1 mm. At such a low particle concentration (but hazardous air traffic operations), the absence of the largest particles in many intermittent ash emissions might explain why these have remained undetected to the radar. In the Rayleigh scattering domain (D bλ/4, see Donnadieu (2012)), where particle sizes are all much less than the radar wavelength (≤5.8 cm at 23.5 cm wavelength), echoes recorded by VOLDORAD 2B are mostly controlled by particle sizes in the upper range of the particle size distribution (PSD). This is true for plumes compound of ash and lapilli only, but becomes untrue as soon as blocks or bombs (≥64 mm, i.e. Mie scattering domain for VOLDORAD 2B) are present because the dependence of the signal amplitude on the particle diameter is not as strong as in the Rayleigh domain. Consequently, VOLDORAD 2B retrieval of mass loading parameters from Strombolian or lava fountaining activity (involving decametric to metric ejecta) requires the full Mie scattering formulation (Gouhier and Donnadieu, 2008).

Among the most critical assumptions for the evaluation of the total mass obtained from radar echo power is the particle size distribution in sounded volumes. The PSD of the deposit is usually evaluated by field data. In literature, there are several methods utilized to determine the PSD of a tephra-fall deposit ranging from simple unweighted averaging of all available grain-size analyses to statistical tools as the Voronoi method. This latter method is constantly applied to PSD analyses of tephra deposits collected soon after explosive events at Etna (Scollo et al., 2007, 2008a, 2008b; Andronico et al., 2008a, 2008b, 2009). However, it is notable that particles dominating the signals at VOLDORAD 2B's wavelength are lapilli and bombs settling early in the vicinity of the vent; as proximal deposits, particularly ballistics, are not often sampled, PSD evaluated by standard approaches are hardly usable to evaluate particle sizes for the analysis of source-targeting radar data. With this aim, comparative analyses of in-situ (plume) PSD could be carried out in the future using measurements from other remote sensing instruments and field data. The size of the largest particles could be assessed by either collecting the very proximal deposits soon after an eruptive event or by analyzing close-up images taken near the vent during the explosive activity.

4.4. Synergetic potential

Measurements from other techniques could be used to crossvalidate radar retrievals. Complementary instruments that naturally combine are the thermal cameras of the video-surveillance system of INGV-OE, also comprising high definition visible cameras, as heat is mainly conveyed by particles and heat flux also depends on particle size and number. They also provide information on volume, height, durations and intensity (e.g., Zanon et al. (2009)). These could be related to radar-inferred parameters like tephra mass and mass flux during lava fountains.

Scanning weather radars like the DPX4 X-band polarimetric radar of the Italian Civil Protection (DPC), located in Catania at 35 km from Etna's summit, can provide very useful information on plume extension, and particle load (Vulpiani et al., 2011; Marzano et al., 2013) and should definitely be compared with VOLDORAD 2B near-source measurements. Being more sensitive to fine ash at centimeter wavelength, it advantageously provides volumetric reflectivity scans with polarimetric information through the whole ash plume at short to medium distance from the source. Thus, there is an obvious synergetic interest to merge the observations of DPX4 with the near-source parameters retrieved from VOLDORAD 2B high rate measurements to retrieve reliable tephra concentration.

Finally, satellite and lidar imagery already used to monitor explosive activity of Etna help to constrain the mass load of the volcanic cloud at medium and distal range (micron-sized particles), by providing the ash mass, ash concentration, particle size, ash thickness (lidar). Integrating these measurements would greatly help to (i) cross-validate tephra concentration and mass measurements, (ii) better understand and model the ascent of ash plumes, particularly the transition from the source up to the neutral buoyancy level and distal dispersal downwind, (iii) improve hazard assessment by providing dispersal models with reliable measured parameters, possibly in near-real-time. Finally, although they do not strictly reflect the particle size distribution inside ash plumes at a given instant, proximal fallout deposits provide essential ground-truth constraints. In particular, the repeated analysis of ground deposits and the continuous monitoring of fallout by disdrometers, either radar- (e.g., Scollo et al (2005)) or laser-based (Scollo et al., 2012), would be of great value.

Acknowledgments

References

Alparone, S., Andronico, D., Sgroi, T., Ferrari, F., Lodato, L., Reitano, D., 2007. Alert system to mitigate tephra fallout hazards at Mt. Etna Volcano, Italy. Nat. Hazards 43, 333–350. http://dx.doi.org/10.1007/s11069-007-9120-7.

Andronico, D., Scollo, S., Cristaldi, A., Caruso, S., 2008a. The 2002–03 Etna explosive activity: tephra dispersal and features of the deposit. J. Geophys. Res. 113, B04209. http://dx.doi.org/10.1029/2007JB005126.

Andronico, D., Cristaldi, A., Scollo, S., 2008b. The 4–5 September 2007 lava fountain at South–East Crater of Mt Etna, Italy. J. Volcanol. Geotherm. Res. 173 (3–4), 325–328. http://dx.doi.org/10.1016/j.jvolgeores.2008.02.004.

Andronico, D., Scollo, S., Cristaldi, A., Ferrari, F., 2009. Monitoring ash emission episodes at Mt. Etna: the 16 November 2006 case study. J. Volcanol. Geotherm. Res. 180 (2–4), 123–134. http://dx.doi.org/10.1016/j.jvolgeores.2008.10.019.

Andronico, D., Lo Castro, M.D., Sciotto, M., Spina, L., 2013. The 2010 ash emissions at the summit craters of Mt Etna: relationship with seismo-acoustic signals. J. Geophys. Res. 118, 1–20. http://dx.doi.org/10.1029/2012JB009895.

Andronico, D., Scollo, S., Cristaldi, A., Lo Castro, M.D., 2014. Representativity of incompletely sampled fall deposits in estimating eruption source parameters: a test using the 12–13 January 2011 lava fountain deposit from Mt. Etna volcano, Italy. Bull. Volcanol. 76, 861. http://dx.doi.org/10.1007/s00445-0140861-3.

Barnard, S.T., 2004. Results of a reconnaissance trip to Mt. Etna, Italy: the effects of the 2002 eruption of Etna on the province of Catania. Bull. N. Z. Soc. Earthq. Eng. 37 (2), 47–62.

Bebbington, M., Cronin, S.J., Chapman, I., Turner, M.B., 2008. Quantifying volcanic ash fall hazard to electricity infrastructure. J. Volcanol. Geotherm. Res. 177, 1055–1062. http://dx.doi.org/10.1016/j.jvolgeores.2008.07.023.

Behncke, B., Branca, S., Corsaro, R.A., De Beni, E., Miraglia, L., Proietti, C., 2014. The 2011–2012 summit activity of Mount Etna: birth, growth and products of the new SE crater. J. Volcanol. Geotherm. Res. 270, 10–21. http://dx.doi.org/10.1016/j.jvolgeores.2013.11.012.

Blong, R.J., 1984. Volcanic Hazards: A Sourcebook on the Effects of Eruptions. Academic Press, Sydney (ISBN: 978-0-12-107180-6).

Boccia, L., Di Massa, G., Venneri, I., 2010. L-band array for ground-based remote sensing of volcanic eruptions. IET Microwaves Antennas Propag. 4 (12), 2062–2068. http://dx.doi.org/10.1049/iet-map.2009.0512.

Bombrun, M., Harris, A., Gurioli, L., Battaglia, J., Barra, V., 2015. Anatomy of a Strombolian eruption: inferences from particle data recorded with thermal video. J. Geophys. Res. Solid Earth 120, 2367–2387. http://dx.doi.org/10.1002/2014JB011556.

Bonaccorso, A., Calvari, S., Linde, A., Sacks, S., 2014. Eruptive processes leading to the most explosive lava fountain at Etna volcano: the 23 November 2013 episode. Geophys. Res. Lett. 41, 4912–4919. http://dx.doi.org/10.1002/2014GL060623.

Branca, S., Del Carlo, P., 2005. Types of eruptions of Etna Volcano AD 1670–2003: Implications for short-term eruptive behavior. Bull. Volcanol. 67, 732–742. http://dx.doi.org/10.1007/s00445-005-0412-z.

Calvari, S., Salerno, G.G., Spampinato, L., Gouhier, M., La Spina, A., Pecora, E., Harris, A.J.L., Labazuy, P., Biale, E., Boschi, E., 2011. An unloading foam model to constrain Etna's 11–13 January 2011 lava fountaining episode. J. Geophys. Res. 116, B11207. http://dx.doi.org/10.1029/2011JB008407.

Chevalier, L., Donnadieu, F., 2015. Considerations on ejection velocity estimations from infrared radiometer data: a case study at Stromboli volcano. J. Volcanol. Geotherm. Res. 302, 130–140. http://dx.doi.org/10.1016/j.jvolgeores.2015.06.022.

Connor, L.G., Connor, C.B., 2006. Inversion is the key to dispersion: understanding eruption dynamics by inverting tephra fallout. In: Mader, H., Cole, S., Connor, C.B. (Eds.), Statistics in Volcanology, Society for Industrial and Applied Mathematics, Special Publication of IAVCEI No. 1. Geological Society, London, pp. 231–242 (ISBN: 978-186239-208-3).

Corsaro, R.A., 2010. Rapporto settimanale sull'attività eruttiva dell'Etna (5–11 aprile 2010), Prot. int. n° UFVG2010/14. URL: http://www.ct.ingv.it/it/comunicati/doc_view/1662-rapporto-settimanale-etna-05-11-aprile-2010.html.

Cronin, S.J., Sharp, D.S., 2002. Environmental impacts on health from continuous volcanic activity at Yasur (Tanna) and Ambrym, Vanuatu. Int. J. Environ. Health Res. 12, 109–123. http://dx.doi.org/10.1080/09603120220129274.

Donnadieu, F., 2012. Volcanological applications of Doppler radars: a review and examples from a transportable pulse radar in L-band. In: Bech, J., Chau, J.L. (Eds.), Doppler Radar Observations — Weather Radar, Wind Profiler, Ionospheric Radar, and Other Advanced Applications, pp. 409–446 http://dx.doi.org/10.5772/35940 (ISBN: 978953-51-0496-4, InTech).

Donnadieu, F., Dubosclard, G., Allard, P., Cordesses, R., Hervier, C., Kornprobst, J., Lénat, J.F., 2003. Sondages des jets volcaniques par radar Doppler: applications à l'Etna. Rapport quadriennal C.N.F.G.G. 1999–2002, pp. 119–124.

Donnadieu, F., Dubosclard, G., Cordesses, R., Druitt, T., Hervier, C., Kornprobst, J., Lénat, J.F., Allard, P., Coltelli, M., 2005. Remotely monitoring volcanic activity with groundbased Doppler radar. Eos. Trans. AGU 86, 204. http://dx.doi.org/10.1029/ 2005EO210001.

Donnadieu, F., Valade, S., Moune, S., 2011. Three dimensional transport speed of winddrifted ash plumes using ground-based radar. Geophys. Res. Lett. 38, L18310. http://dx.doi.org/10.1029/2011GL049001.

Donnadieu, F., Freville, P., Rivet, S., Hervier, C., Cacault, P., 2015. The Volcano Doppler Radar Data Base of Etna (VOLDORAD 2B). Online data base, 2009–. OPGC ClermontFerrand: Université Clermont Auvergne – CNRS http://dx.doi.org/10.18145/VOLDORAD.ETNA.2009 (http://wwwobs.univ-bpclermont.fr/SO/televolc/voldorad/bddtr.php).

Dubosclard, G., Cordesses, R., Allard, P., Hervier, C., Coltelli, M., Kornprobst, J., 1999. First testing of a volcano Doppler radar (Voldorad) at Mt. Etna. Geophys. Res. Lett. 26, 3389–3392.

Dubosclard, G., Donnadieu, F., Allard, P., Cordesses, R., Hervier, C., Coltelli, M., Privitera, E., Kornprobst, J., 2004. Doppler radar sounding of volcanic eruption dynamics at Mount Etna. Bull. Volcanol. 66, 443–456. http://dx.doi.org/10.1007/s00445-003-0324-8.

Elbern, H., Broad, A., Engelen, R., Husson, P., Scollo, S., Seibert, P., Stohl, A., Tait, S., Thordarson, T., Varghese, S., 2010. How can the R&D community best contribute to improve VAAC analysis and prediction of volcanic ash plume? Monitoring Volcanic Ash from Space ESA-EUMETSAT Workshop on the 14 April to 23 May 2010 Eruption at the Eyjafjöll Volcano, South Iceland

Gaudin, D., Taddeucci, J., Scarlato, P., Moroni, M., Freda, C., Gaeta, M., Palladino, D.M., 2014. Pyroclast tracking velocimetry illuminates bomb ejection and explosion dynamics at Stromboli (Italy) and Yasur (Vanuatu) volcanoes. J. Geophys. Res. Solid Earth 119, 5384–5397. http://dx.doi.org/10.1002/2014JB011096.

Gouhier, M., Donnadieu, F., 2008. Mass estimations of ejecta from Strombolian explosions by inversion of Doppler radar measurements. J. Geophys. Res. 113, B10202. http://dx.doi.org/10.1029/2007JB005383.

Gouhier, M., Donnadieu, F., 2010. The geometry of Strombolian explosions: insight from Doppler radar measurements. Geophys. J. Int. 183, 1376–1391. http://dx.doi.org/10.1111/j.1365-246X.2010.04829.x.

Gouhier, M., Donnadieu, F., 2011. Systematic retrieval of ejecta velocities and gas fluxes at Etna volcano using L-band Doppler radar. Bull. Volcanol. 73 (9), 1139–1145. http://dx.doi.org/10.1007/s00445-011-0500-1.

Gouhier, M., Harris, A.J.L., Calvari, S., Labazuy, P., Guéhenneux, Y., Donnadieu, F., Valade, S., 2012. Lava discharge during Etna's January 2011 fire fountain tracked using MSGSEVIRI. Bull. Volcanol. 74, 787–793. http://dx.doi.org/10.1007/s00445-011-0572-y.

Guffanti, M., Mayberry, G.C., Casadevall, T.J., Wunderman, R., 2009. Volcanic hazards to airports. Nat. Hazards 51, 287–302. http://dx.doi.org/10.1007/s11069-008-9254-2.

Guffanti, M., Casadevall, T.J., Budding, K., 2010. Encounters of aircraft with volcanic ash clouds; a compilation of known incidents, 1953–2009. U.S. Geological Survey Data Series, 545, ver. 1.0, p. 12 (URL: http://pubs.usgs.gov/ds/545/DS545.pdf).

Harris, A.J.L., Ripepe, M., Hughes, E., 2012. Detailed analysis of particle launch velocities, size distributions and gas densities during normal explosions at Stromboli. J. Volcanol. Geotherm. Res. 231-232, 109–131. http://dx.doi.org/10.1016/j. jvolgeores.2012.02.012.

Harris, A.J.L., Valade, S., Sawyer, G., Donnadieu, F., Battaglia, J., Gurioli, L., Kelfoun, K., Labazuy, P., Stachowicz, T., Bombrun, M., Barra, V., Delle Donne, D., Lacanna, G., 2013. Modern multispectral sensors help track explosive eruptions. Eos 94 (37), 321–322.

INGV- Rep. N° 35/2010, 2016d. Bollettino settimanale sul monitoraggio vulcanico, geochimico e sismico del vulcano Etna, 23/08/2010–29/08/2010 URL: http://www.ct.ingv.it/it/comunicati/doc_view/2063-bollettino-settimanale-sul-monitoraggiovulcanico-geochimico-e-sismico-del-vulcano-etna-31-08-2010.html.

Lo Castro, 2010. Rapporto settimanale sull'attività eruttiva dell'Etna (16–22 novembre 2009), Prot. int. n° UFVG2009/87. http://www.ct.ingv.it/en/avvisi-e-bandi/doc_ download/1220-rapporto-settimanale-etna-16-22-novembre-2009.html.

Marzano, F.S., Picciotti, E., Montopoli, M., Vulpiano, G., 2013. Inside volcanic clouds. Remote Sensing of ash plumes using microwave weather radars. Bull. Am. Meteorol. Soc. 94, 1567–1586. http://dx.doi.org/10.1175/BAMS-D-11-00160.1.

Mora, M.M., Lesage, P., Donnadieu, F., Valade, S., Schmidt, A., Soto, G., Taylor, W., Alvarado, G., 2009. Joint seismic, acoustic and Doppler radar observations at Arenal Volcano, Costa Rica: preliminary results. In: Bean, C.J., Braiden, A.K., Lokmer, I., Martini, F., O'Brien, G.S. (Eds.), VOLUME Project, EU PF6 (No. 018471), P.330–340. VOLUME Project Consortium, Dublin, p. 348 (ISBN 978-1-905254-39-2).

Prata, F., Bluth, G., Rose, B., Schneider, D., Tupper, A., 2001. Comments on "failures in detecting volcanic ash from a satellite-based technique". Remote Sens. Environ. 78, 341–346. http://dx.doi.org/10.1016/S0034-4257(01)00231-0.

Scharff, L., Ziemen, F., Hort, M., Gerst, A., Johnson, J.B., 2012. A detailed view into the eruption clouds of Santiaguito volcano, Guatemala, using Doppler radar. J. Geophys. Res. 117, B04201. http://dx.doi.org/10.1029/2011JB008542.

Scollo, S., Coltelli, M., Prodi, F., Folegani, M., Natali, S., 2005. Terminal settling velocity measurements of volcanic ash during the 2002–2003 Etna eruption by an X-band microwave rain gauge disdrometer. Geophys. Res. Lett. 32, L10302. http://dx.doi.org/10.1029/2004GL022100.

Scollo, S., Del Carlo, P., Coltelli, M., 2007. Tephra fallout of 2001 Etna flank eruption: analysis of the deposit and plume dispersion. J. Volcanol. Geotherm. Res. 160, 147–164. http://dx.doi.org/10.1016/j.jvolgeores.2006.09.007.

Scollo, S., Folch, A., Costa, A., 2008a. A parametric and comparative study on different tephra fallout models. J. Volcanol. Geotherm. Res. 176, 199–211. http://dx.doi.org/10.1016/j.jvolgeores.2008.04.002.

Scollo, S., Tarantola, S., Bonadonna, C., Coltelli, M., Saltelli, A., 2008b. Sensitivity analysis and uncertainty estimation for tephra dispersal models. J. Geophys. Res. 113, B06202. http://dx.doi.org/10.1029/2006JB004864.

Scollo, S., Prestifilippo, M., Spata, G., D'Agostino, M., Coltelli, M., 2009. Forecasting and monitoring Etna volcanic plumes. Nat. Hazards Earth Syst. Sci. 9, 1573–1585.

Scollo, S., Boselli, A., Coltelli, M., Leto, G., Pisani, G., Spinelli, N., Wang, X., 2012. Monitoring Etna volcanic plumes using a scanning Lidar. Bull. Volcanol. 74, 2382–2395. http://dx.doi.org/10.1007/s00445-012-0669-y.

Scollo, S., Coltelli, M., Bonadonna, C., Del Carlo, P., 2013. Tephra hazard assessment at Mt. Etna (Italy). Nat. Hazards Earth Syst. Sci. 13, 3221–3233. http://dx.doi.org/10.5194/ nhess-13-3221-2013.

Stevenson, J.A., Millington, S.C., Beckett, F.M., Swindles, G.T., Thordarson, T., 2015. Big grains go far: understanding the discrepancy between tephrochronology and satellite infrared measurements of volcanic ash. Atmos. Meas. Tech. 8, 2069–2091. http://dx.doi.org/10.5194/amt-8-2069-2015.

Taddeucci, J., Scarlato, P., Capponi, A., Del Bello, E., Cimarelli, C., Palladino, D.M., Kueppers, U., 2012. High-speed imaging of Strombolian explosions: the ejection velocity of pyroclasts. Geophys. Res. Lett. 39, L02301. http://dx.doi.org/10.1029/2011GL050404. Valade, S., Donnadieu, F., 2011. Ballistics and ash plumes discriminated by Doppler radar. Geophys. Res. Lett. 38, L22301. http://dx.doi.org/10.1029/2011GL049415.

Valade, S., Donnadieu, F., Lesage, P., Mora, M.M., Harris, A., Alvarado, G.E., 2012. Explosion mechanisms at Arenal volcano, Costa Rica: an interpretation from integration of seismic and Doppler radar data. J. Geophys. Res. 117, B01309. http://dx.doi.org/10.1029/ 2011JB008623.

Vulpiani, G., Montopoli, M., Picciotti, E., Marzano, F.S., 2011. On the use of a polarimetric X-band weather radar for volcanic ash clouds monitoring. 35th Conference on radar meteorology, Pittsburgh, PA, USA.

Wardman, J.B., Wilson, T.M., Bodger, P.S., Cole, J.W., Johnston, D.M., 2012. Investigating the electrical conductivity of volcanic ash and its effect on HV power systems. Phys. Chem. Earth 45-46, 128–145. http://dx.doi.org/10.1016/j.pce.2011.09.003.

Webley, P.W., Stunder, B.J.B., Dean, K.G., 2009. Preliminary sensitivity study of eruption source parameters for operational volcanic ash cloud transport and dispersion models — a case study of the August 1992 eruption of the crater peak vent, Mount Spurr, Alaska. J. Volcanol. Geotherm. Res. 186 (1–2), 108–119. http://dx.doi.org/10. 1016/j.jvolgeores.2009.02.012.

Zanon, V., Neri, M., Pecora, E., 2009. Interpretation of data from the monitoring thermal camera of Stromboli volcano (Aeolian Islands, Italy). Geol. Mag. 146 (4), 591–601. http://dx.doi.org/10.1017/S0016756809005937.